

Multicolor Quantum Metrology with Entangled Photons

Bryn Bell,¹ Srikanth Kannan,¹ Alex McMillan,¹ Alex S. Clark,² William J. Wadsworth,³ and John G. Rarity^{1,*}

¹*Department of Electrical and Electronic Engineering, Centre for Quantum Photonics,
University of Bristol, Bristol BS8 1UB, United Kingdom*

²*Centre for Ultrahigh bandwidth Devices for Optical Systems (CUDOS), Institute of Photonics and Optical Science,
University of Sydney, New South Wales 2006, Australia*

³*Department of Physics, Centre for Photonics and Photonic Materials, University of Bath, Bath BA2 7AY, United Kingdom*

(Received 31 May 2013; published 29 August 2013)

Entangled photons can be used to make measurements with an accuracy beyond that possible with classical light. While most implementations of quantum metrology have used states made up of a single color of photons, we show that entangled states of two colors can show supersensitivity to optical phase and path length by using a photonic crystal fiber source of photon pairs inside an interferometer. This setup is relatively simple and robust to experimental imperfections. We demonstrate sensitivity beyond the standard quantum limit and show superresolved interference fringes using entangled states of two, four, and six photons.

DOI: [10.1103/PhysRevLett.111.093603](https://doi.org/10.1103/PhysRevLett.111.093603)

PACS numbers: 42.50.Dv, 03.67.Bg

The measurement of phase in an interferometer is a consequence of the wavelike nature of light, while the uncertainty in that measurement comes from the particle nature of light, revealed in the detection process. This single photon nature of interference was first noted by Taylor's experiment of 1909 [1] while Dirac, in his book on quantum mechanics [2], went as far as to say "each photon then interferes only with itself." Seminal experiments have since shown that this description is too restrictive [3], and that two photon interference is a valid phenomenon [4]. However, multiphoton interferometry experiments aimed at metrology [5,6] can shed further light on Dirac's statement. Here, we investigate interferometry with states comprising pairs of photons of distinct wavelengths emitted into one arm or the other of an interferometer. Each photon is detected by a wavelength selective detector and can only have interfered with itself. The correlations between photons ensure that stable interference fringes are only seen when photons are detected in coincidence, with the fringe spacing roughly half their mean wavelength. We extend this superresolution to four and six photon detections, achieving a fringe spacing one-sixth of the original pumping beam wavelength. Subtly, quantum interference between separate photons does play a part in the four and six photon experiments and can affect the shape and contrast of the fringes.

The uncertainty in measuring an optical phase θ with an interferometer is limited by Poissonian statistical uncertainty (or shot noise) in the discrete number of photons detected. In classical experiments this standard quantum limit (SQL) on measurement precision is $\Delta\theta \geq 1/\sqrt{N}$, with N the total number of photons detected. In principle, using quantum resources it is possible to dramatically improve on the SQL and reach the Heisenberg limit $\Delta\theta \geq 1/N$ [7]. This has particular applications when the sample

has a low damage threshold and it is necessary to extract the maximum possible information without exposing the sample to high intensity illumination.

In our experiment, we show potential improvements over the SQL with a setup which overcomes two practical drawbacks common to previous implementations of quantum metrology:

(1) Generating entanglement by Hong-Ou-Mandel (HOM) interference, as in Fig. 1(a), is technically demanding and highly sensitive to any distinguishability between the photons [4,5]. Indistinguishability is usually achieved using narrow filtering, at a cost to the transmission efficiency [8]. The phase sensitivity of entangled states tends to be highly sensitive to loss, and filtering all photon channels largely cancels out the quantum advantage [9]. By generating path entanglement as shown schematically in Fig. 1(b), using a source of photon pairs in each interferometer arm, the SQL can be beaten without the need for HOM interference between indistinguishable photons. No quantum resources are required as inputs to the interferometer, only a classical laser.

(2) Using a parametric down-conversion source of photons implies that a bright coherent pump beam of half the wavelength is available [10–12]. While entangling two down-converted photons can result in an enhanced precision in terms of a phase, they perform no better than the pump laser at measuring a path length, as shown below. By using four-wave mixing (FWM) in photonic crystal fiber (PCF) we produce nondegenerate pairs of photons with the signal and idler equally spaced above and below the pump beam in frequency, so that the central frequency is unchanged and an advantage in length sensitivity is seen using two photon states.

For a given quantum state, the maximum sensitivity to a general parameter x can be calculated from the quantum

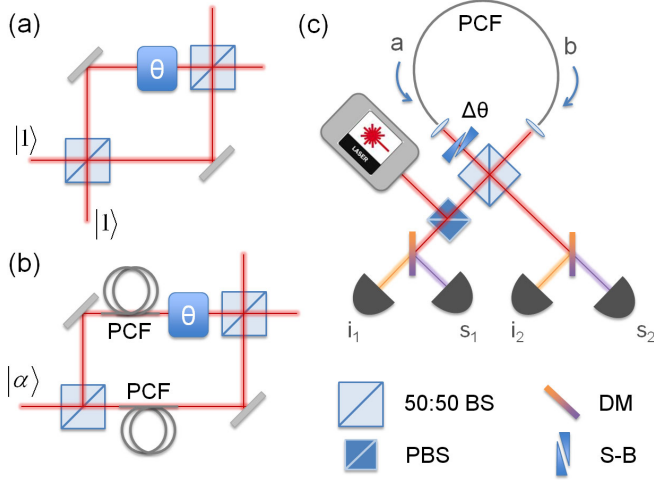


FIG. 1 (color online). Generation of entangled states for enhanced measurement of θ (a) by HOM interference between two single photons, (b) by a bright coherent state α , which pumps two identical PCF pair-photon sources inside the interferometer. The two methods result in equivalent states, except that in (b) the photon pairs do not need to be degenerate in wavelength. (c) Experimental setup using one fiber source of nondegenerate photon pairs pumped in two directions. BS: beam splitter; PBS: polarizing beam splitter; DM: dichroic mirror; S-B: Soleil-Babinet compensator.

Cramér-Rao bound [13,14], so that assuming a pure state and unitary evolution

$$\Delta x \geq \frac{1}{2\sqrt{\nu}\Delta\hat{H}_x}. \quad (1)$$

Here ν is the number of copies of the state used and $\Delta\hat{H}_x$ is the spread of an operator \hat{H}_x , a Hamiltonian analogue describing the effect of the parameter on the state such that $|\psi\rangle \rightarrow e^{-i\hat{H}_x x}|\psi\rangle$. For a phase θ applied to a mode, $\hat{H}_\theta = \hat{n}$, the photon number operator for that mode. Since we are considering multiple wavelengths, which will experience different phase shifts from a particular sample, a more appropriate choice of parameter is the optical path length L (an actual length multiplied by a refractive index—we will assume the sample is dispersionless here for simplicity). \hat{H}_x has to be adjusted for this change of parameter and for the presence of multiple modes with frequencies ω_k and number operators \hat{n}_k :

$$\hat{H}_L = \sum_k \frac{\omega_k \hat{n}_k}{c}. \quad (2)$$

This is proportional to the total energy summed over all wavelengths. Hence we can evaluate the usefulness of a state $|\psi\rangle$ in measuring L from Eq. (1) by using

$$\Delta H_L^2 = \langle \psi | H_L^2 | \psi \rangle - (\langle \psi | H_L | \psi \rangle)^2. \quad (3)$$

For N uncorrelated photons of the same frequency, split equally between the sample arm a and a reference arm b of an interferometer,

$$\Delta L \geq \frac{c}{\omega\sqrt{N}}, \quad (4)$$

showing SQL scaling with a frequency dependence. This expression potentially exaggerates the benefits of using a higher frequency, because as well as showing higher sensitivity, this might be expected to cause more damage to the sample. Rewriting in terms of the total energy detected rather than the number of photons, $E = N\hbar\omega$, we find that for a given energy through the interferometer, higher frequency photons still perform better:

$$\Delta L \geq \left(\frac{c^2\hbar}{\omega E}\right)^{1/2}. \quad (5)$$

Using NOON states, maximally correlated states of m photons where $m \ll N$, a \sqrt{m} improvement is possible [6]. Hence an entangled pair of photons ($m = 2$) gives the same information per energy as a coherent state of twice the frequency (2ω and $m = 1$). However, an entangled pair of photons at $\omega \pm \Delta\omega$ can retain a $\sqrt{2}$ advantage over a coherent state with frequency ω .

The proof of principle experiment shown in Fig. 1(c) makes use of a Sagnac interferometer to provide intrinsic stability between the clockwise and counterclockwise paths [15–19]. Spontaneous FWM in a length of birefringent PCF produces nondegenerate pairs of photons at 625 and 860 nm in both paths when pumped in both directions by picosecond laser pulses at 720 nm. Conditional on a single pair being generated, the two photon state can be written as

$$|\psi_2\rangle = \frac{1}{\sqrt{2}}(|10\rangle_s |10\rangle_i - e^{2i\theta_p} |01\rangle_s |01\rangle_i). \quad (6)$$

The subscripts s , i , and p denote signal, idler, and pump wavelengths and the kets $|a, b\rangle$ contain the number of photons in interferometer paths a and b . Energy conservation in the FWM mixing process requires that $2\omega_p = \omega_s + \omega_i$. The state evolves with a summed phase $2\theta_p = \theta_s + \theta_i = L(\omega_s + \omega_i)/c$. A variable birefringent element allows control of this phase [20]. The paths are combined at a broadband 50:50 beam splitter, and at each output the signal and idler modes are separated with dichroic mirrors then detected using silicon avalanche photodiodes.

Classical interference can be observed between the pump light in the two paths [Fig. 2(a)]. Two photon coincidence detections corresponding to the state $|\psi_2\rangle$ then oscillate as predicted by theory between the bunched and antibunched cases (signal and idler emerge from the same or different outputs, respectively) in an interference fringe with half the period of the classical case, shown in Fig. 2(b). Note that if chromatic dispersion in the sample caused the signal, idler, and pump wavelengths to experience significantly different refractive indices, the period of the two fringes would not be related by an exact factor of 2. Despite the relatively large range of wavelengths used, this factor is seen to be 2 here, in agreement with calculations from the Sellmeier equations for quartz, which predict a deviation of less than 1% [21].

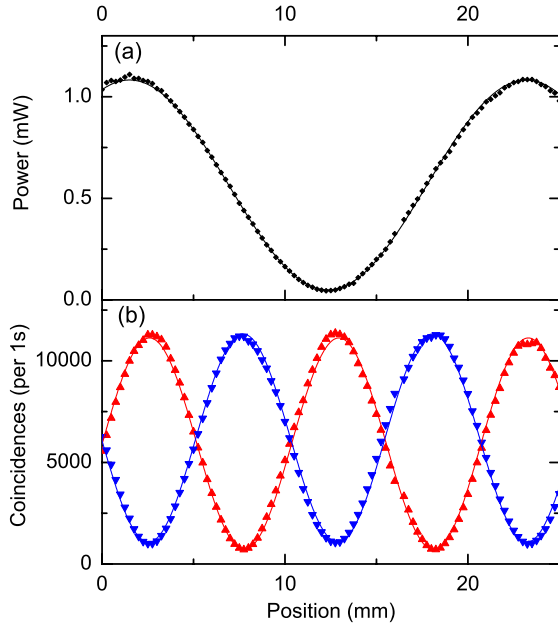


FIG. 2 (color online). (a) Classical interference with the pump beam at 720 nm as the position of the Soleil-Babinet compensator is varied and (b) two-photon interference with half the period (red upward pointing triangles: bunched coincidences; blue downward triangles: antibunched). Both with sinusoidal fit lines.

The visibility of the classical interference is $\sim 92\%$ and mainly limited by different coupling efficiencies through the PCF in the two directions resulting in incomplete cancellation. The two-photon visibility is $\sim 88\%$, and is affected to a greater extent by any unmatched coupling efficiencies or losses, as well as background contributions from higher-order photon emission. This is well above the usual threshold of $\sqrt{0.5} \approx 70.7\%$ to demonstrate sensitivity better than the SQL [10] and corresponds to an uncertainty ΔL of 0.8 times the SQL. Note that this improvement and the form of the interference fringes are unaffected if spectral correlations are present between signal and idler, leading to them being detected individually in a mixed state. This is an advantage over implementations involving HOM interference to produce entanglement, though in our experiment it is necessary to avoid spectral correlations in order to see any additional improvement from using higher-photon-number states [19].

The two-photon detections also suggest that the beam splitter is acting as a nonunitary operation at the signal wavelength, resulting in some additional phase shifts between interfering terms [19]. These were taken into account in the theoretical four- and six-photon curves.

When two signal-idler pairs are created in the PCF, the four-photon wave function can be written as

$$|\psi_4\rangle = \frac{1}{\sqrt{3}}(|20\rangle_s|20\rangle_i - e^{2i\theta_p}|11\rangle_s|11\rangle_i + e^{4i\theta_p}|02\rangle_s|02\rangle_i). \quad (7)$$

Unlike $|\psi_2\rangle$, this behaves differently to a NOON state due to the middle term in the superposition, involving one pair

being created in each path—in a NOON state, the photons are either all in one path or all in the other. $|\psi_4\rangle$ bears more similarity to a Holland-Burnett state [22]. In ideal conditions Holland-Burnett states show sensitivity above the SQL but below that of a NOON state, and are an attractive route to entanglement-enhanced metrology because they are simple to generate for arbitrary N and show a better tolerance to photon loss.

Figure 3 shows fringes observed when monitoring (at separate times) three different four-photon coincidence detections across the outputs of the interferometer. The fringes in Figs. 3(a) and 3(b) are approximately sinusoidal with $1/4$ the period of the classical fringe, a characteristic of a four-photon NOON state. This is because HOM interference acts on the middle term in $|\psi_4\rangle$ and causes the signal photons to bunch together after the final beam splitter, so that if the two signal photons are detected at separate outputs, they must have come from one of the other two components of the state, which together resemble a NOON state [10]. The same argument applies to detecting the two idler photons at separate outputs, so that any detection pattern involving like photons at separate outputs is expected to show sinusoidal interference with fourfold superresolution. Conversely, for detection patterns with both signals at the same output and both

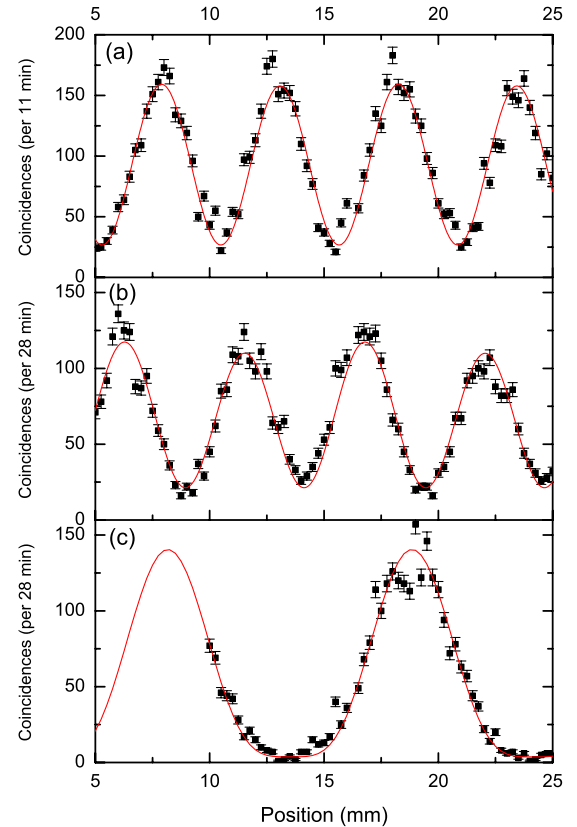


FIG. 3 (color online). Fourfold counts for (a) the $|11\rangle_s|11\rangle_i$ output, (b) the $|20\rangle_s|11\rangle_i$ output, and (c) the $|20\rangle_s|02\rangle_i$ output. Fit lines are based on calculation [19].

idlers at the same output, the middle term will have an increased effect due to bunching. As seen in Fig. 3(c), the effect is a curve with twofold superresolution, with some flattening at the minima and sharpening at the maxima due to the presence of a fourfold component. This curve is more tolerant to loss, as can be seen from its high visibility compared to (a) and (b), which is expected for interference using a Holland-Burnett-like state. Note that the $|20\rangle_s|11\rangle_i$ fringe in Fig. 3(b) corresponds directly to the $|31\rangle$ output in the one color case [10], and similarly it can still show fourfold superresolution with full visibility if separate photon pairs are distinguishable and act independently, in which case the state would be described by $|\psi_2\rangle \otimes |\psi'_2\rangle$ rather than $|\psi_4\rangle$. However, the $|11\rangle_s|11\rangle_i$ fringe in Fig. 3(a) does not have an analogue in one color experiments, and if multiphoton interference did not take place between signals from separate pairs or idlers from separate pairs the visibility would be limited to 33%. Hence this fringe acts as a test of multiphoton interference taking place and demonstrates that the four photon state can show improved sensitivity compared to multiple two photon states.

We have measured fringes in only three out of the nine possible detection patterns for $|\psi_4\rangle$ —after the beam splitter operation, the signal photons can be detected in three states, $|20\rangle$, $|11\rangle$, or $|02\rangle$, which are multiplied by the same three possibilities for the idler photons—but it is in principle possible to monitor all output states simultaneously. This would clearly allow better sensitivity since all the output states provide information about the phase. As described in [10], when calculating the sensitivities from individual fringes, the visibility and the intrinsic detection efficiency of the fringe should be taken into account, as well as its gradient. For the fringes in Figs. 3(a)–3(c), we find values for ΔL of 1.18, 1.82, and 1.75, respectively, relative to the SQL. No individual fringe beats the SQL, due to the nonunit visibilities, and because the state is divided between more potential detection patterns than in the single color case. However, adding the Fisher information [7] from separate fringes suggests they would allow an improvement if they were monitored simultaneously. Since of the six outputs we did not measure we expect three to be of the same form as (b) and three the same form as (c), we can estimate that monitoring all nine outputs would give a minimum uncertainty 0.72 of the SQL. This would be a significant improvement over the SQL, though it is still above the theoretical value from Eq. (1) for $|\psi_4\rangle$ of 0.61 due to the nonunit visibilities, and above the Heisenberg limit for four photons of 0.5.

A general wave function for m photons of two colors can be written as [19]

$$|\psi_m\rangle = \sum_{r=0}^{m/2} \frac{(-1)^r e^{2ir\theta_p}}{\sqrt{\frac{m}{2} + 1}} |m/2 - r, r\rangle_s |m/2 - r, r\rangle_i. \quad (8)$$

For example, $m = 6$ leads to

$$|\psi_6\rangle = \frac{1}{2} \left(\begin{array}{l} |30\rangle_s|30\rangle_i - e^{2i\theta_p}|21\rangle_s|21\rangle_i \\ + e^{4i\theta_p}|12\rangle_s|12\rangle_i - e^{6i\theta_p}|03\rangle_s|03\rangle_i \end{array} \right). \quad (9)$$

Figure 4 shows an example of $|\psi_6\rangle$ with the detection pattern $|21\rangle_s|21\rangle_i$, which is expected to contain oscillation at both 2 and 6 times the classical frequency. Multiphoton interference again plays a part—if separate photon pairs were distinguishable, only twofold oscillation would remain. The data are in good agreement with theory, though there is a high level of background noise from higher-order emission due to the high pump power used and the low count rate. It is clear that the data taken do not achieve the 82% visibility required to exceed the SQL; however, improvements in the level and balancing of collection and detection efficiencies would bring us towards this goal.

$|\psi_m\rangle$ is an equally weighted superposition of all distributions of $m/2$ signal-idler pairs between the two paths, with each path necessarily containing equal numbers of signal and idler photons. This results in simple expressions for Eqs. (2) and (3) [19], leading to a minimum uncertainty in L given by

$$\Delta L \geq \left(\frac{3c^2\hbar}{\omega_p E(m+4)} \right)^{1/2}. \quad (10)$$

Hence, for a general two color entangled state the shot noise will scale below the SQL by a factor $\sqrt{(m+4)/3}$, potentially achieving significant improvements at large m . With current technology, detecting large numbers of coincident photons is impractical due to the relatively low efficiency of single photon detectors, and the improved sensitivity of the state drops rapidly with any form of loss including imperfect detectors. Although an analysis of loss tolerance is beyond the scope of this Letter, the similarity of these states to Holland-Burnett states suggests that they will fare better than NOON states. Also note that

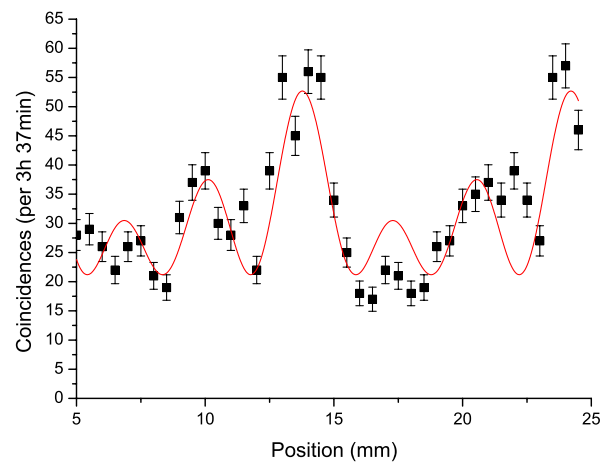


FIG. 4 (color online). Sixfold coincidences in the $|21\rangle_s|21\rangle_i$ output with a fit line based on theory.

the states are generated spontaneously by the source, so that it is not possible to obtain a high sensitivity m photon entangled state on demand. Rather, we expect that in a low loss setting, increasing the pair generation rate of the source will improve sensitivity as more high- m states occur, unlike the current situation where a higher generation rate tends to add noise to the results.

In conclusion, we have shown that two color entangled states could be a useful resource for quantum metrology and demonstrate these effects up to six photon states in a novel ultrastable interferometer. We have seen that single photon interference *and* multiphoton interference combine to increase the visibility of fringes at the four and six photon level, and ultimately lead to improved sensitivity. When lumped losses are reduced giving access to entangled states consisting of larger numbers of photons, the simplicity of this path-entangled pair photon source and its improved sensitivity to path length make it a promising approach to future quantum metrology and enhanced sensing.

We acknowledge support from U.K. EPSRC, EU Grants No. 248905 Q-Essence and No. 600838 QWAD, ERC Grant No. 247462 QUOWSS, and the Australian Research Council Centre of Excellence (CUDOS, CE110001018) and DECRA (DE130101148) schemes.

*john.rarity@bristol.ac.uk

- [1] G. I. Taylor, Proc. Cambridge Philos. Soc. **15**, 114 (1909).
- [2] P. A. M. Dirac, *Quantum Mechanics* (Oxford University, London, 1958), 4th ed., Chap. I, p. 9.
- [3] R. L. Pfleeger and L. Mandel, *Phys. Rev.* **159**, 1084 (1967).
- [4] C. K. Hong, Z. Y. Ou, and L. Mandel, *Phys. Rev. Lett.* **59**, 2044 (1987).
- [5] J. G. Rarity, P. R. Tapster, E. Jakeman, T. Larchuk, R. A. Campos, M. C. Teich, and B. E. A. Saleh, *Phys. Rev. Lett.* **65**, 1348 (1990).
- [6] J. Dowling, *Contemp. Phys.* **49**, 125 (2008).
- [7] V. Giovannetti, S. Lloyd, and L. Maccone, *Science* **306**, 1330 (2004).
- [8] E. Pomarico, B. Sanguinetti, C. I. Osorio, H. Herrmann, and R. T. Thew, *New J. Phys.* **14**, 033008 (2012).
- [9] R. Demkowicz-Dobrzanski, U. Dorner, B. J. Smith, J. S. Lundeen, W. Wasilewski, K. Banaszek, and I. A. Walmsley, *Phys. Rev. A* **80**, 013825 (2009).
- [10] T. Nagata, R. Okamoto, J. L. O'Brien, K. Sasaki, and S. Takeuchi, *Science* **316**, 726 (2007).
- [11] J. C. F. Matthews, A. Politi, D. Bonneau, and J. L. O'Brien, *Phys. Rev. Lett.* **107**, 163602 (2011).
- [12] G. Y. Xiang, B. L. Higgins, D. W. Berry, H. M. Wiseman, and G. J. Pryde, *Nat. Photonics* **5**, 43 (2010).
- [13] V. Giovannetti, S. Lloyd, and L. Maccone, *Nat. Photonics* **5**, 222 (2011).
- [14] S. Luo, *Lett. Math. Phys.* **53**, 243 (2000).
- [15] X. Li, P. L. Voss, J. E. Sharping, and P. Kumar, *Phys. Rev. Lett.* **94**, 053601 (2005).
- [16] J. Fulconis, O. Alibart, J. L. O'Brien, W. J. Wadsworth, and J. G. Rarity, *Phys. Rev. Lett.* **99**, 120501 (2007).
- [17] A. Clark, B. Bell, J. Fulconis, M. M. Halder, B. Cerny, O. Alibart, C. Xiong, W. J. Wadsworth, and J. G. Rarity, *New J. Phys.* **13**, 065009 (2011).
- [18] A. Fedrizzi, T. Herbst, A. Poppe, T. Jennewein, and A. Zeilinger, *Opt. Express* **15**, 15377 (2007).
- [19] See Supplemental Material at <http://link.aps.org/supplemental/10.1103/PhysRevLett.111.093603> for additional experimental details and derivations of the state vectors and optimal sensitivities.
- [20] M. Halder, J. Fulconis, B. Cerny, A. Clark, C. Xiong, W. J. Wadsworth, and J. G. Rarity, *Opt. Express* **17**, 4670 (2009).
- [21] Thorlabs Soleil Babinet Compensator User Guide, <http://www.thorlabs.de/Thorcat/6500/SBC-VIS-Manual.pdf>.
- [22] M. J. Holland and K. Burnett, *Phys. Rev. Lett.* **71**, 1355 (1993).